Hierarchical Cobalt-Pentlandite (Co, Ni, Zn)$_9$S$_8$ Nanostructures: Advanced Electrodes for Flexible Solid-State Supercapacitors

Ye Tian[a,b], Ning Liu[a,b], Qian Xue[b], Hao Liu[a*], Xueqiang Qi[c*], Andreu Cabot[b, d], Libing Liao[e*]

[a] *School of Science, China University of Geosciences, Beijing 100083, P. R. China*
Email: liuhao1398@cugb.edu.cn

[b] *Catalonia Institute for Energy Research–IREC, Sant Adrià de Besòs, Barcelona 08930, Spain*

[c] *College of Chemistry and Chemical Engineering, Chongqing University of Technology, Chongqing 400054, China*
Email: xqqi@cqut.edu.cn

[d] *Catalan Institution for Research and Advanced Studies–ICREA, Pg. Lluís Companys 23, Barcelona 08010, Spain*

[e] *Engineering Research Center of Ministry of Education for Geological Carbon Storage and Low Carbon Utilization of Resources, Beijing Key Laboratory of Materials Utilization of Nonmetallic Minerals and Solid Wastes, School of Materials Science and Technology, China University of Geosciences (Beijing), Beijing 100083, China*
Email: lbliao@cugb.edu.cn

Figures:

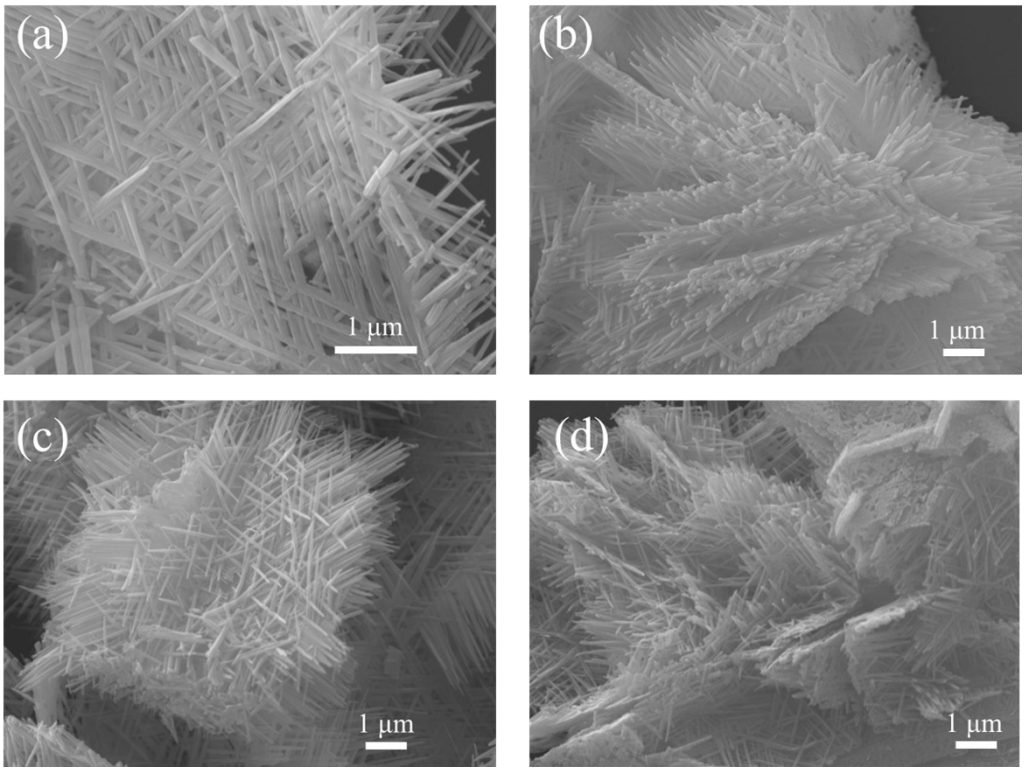

Figure S1. SEM image of (a) CNZS-1; (b) CNZS-2; (c) CNZS-3; (d) CNZS-4.

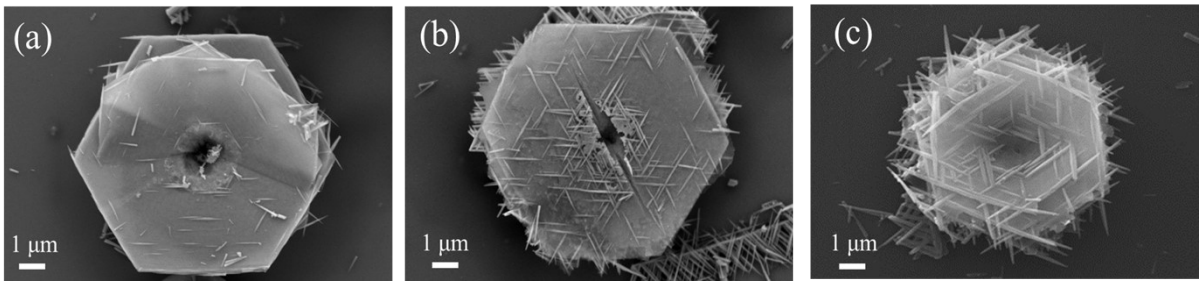

Figure S2. SEM images of CNZS-3 obtained at different reaction times during the second-step hydrothermal process: (a) 0.5 h; (b) 3 h; and (c) 9 h.

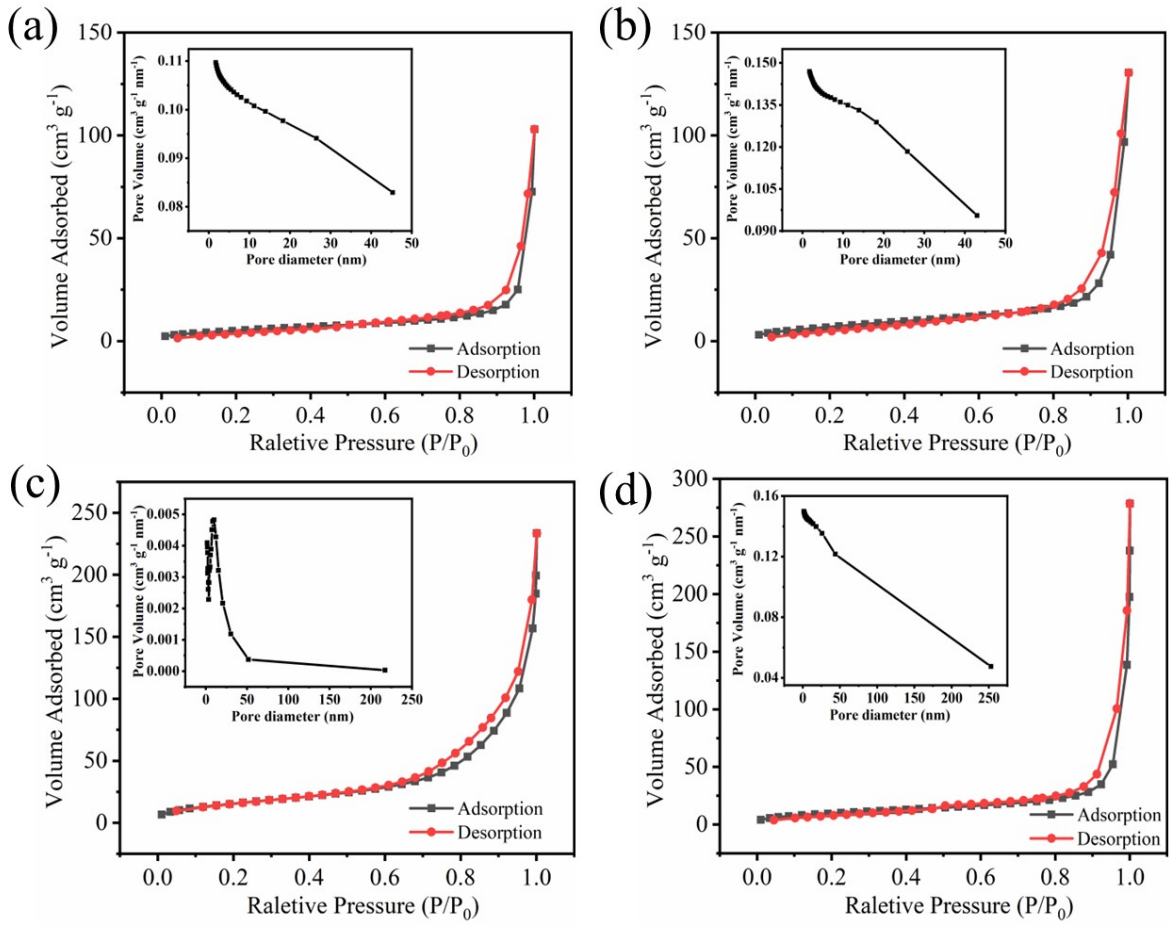

Figure S3. Nitrogen adsorption-desorption isotherms of (a) CNZS-1; (b) CNZS-2; (c) CNZS-3; (d) CNZS-4. Insets show the corresponding pore size distribution curves.

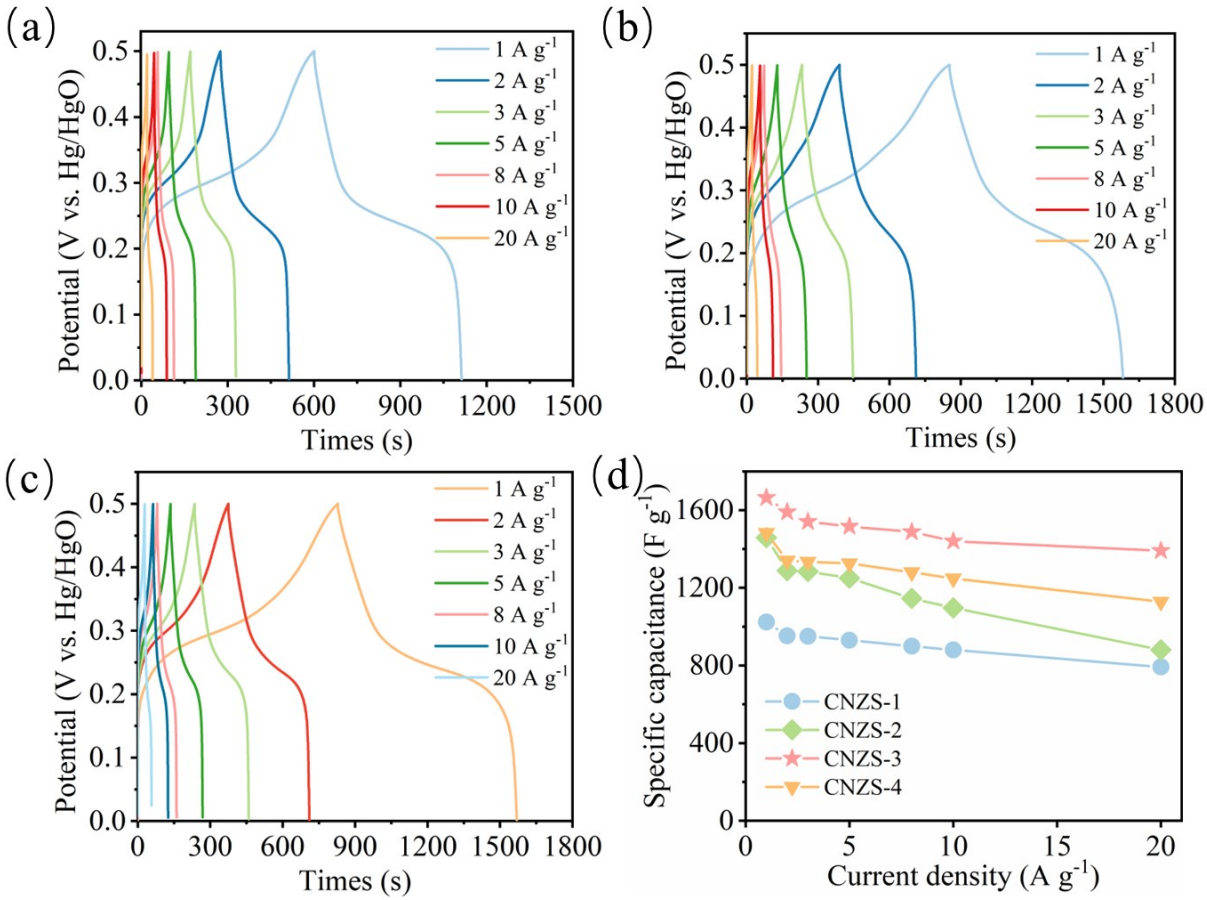

Figure S4. (a-c) GCD curves of (a) CNZS-1, (b) CNZS-2, and (c) CNZS-4 at different current densities; (d) Rate performance of CNZS at 1-20 A g^{-1}.

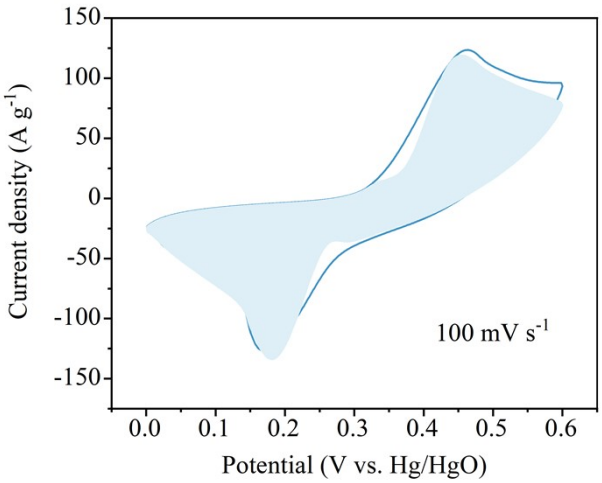

Figure S5. Pseudocapacitance contribution (blue region) in CV curve of CNZS-3 at 100 mV s^{-1}.

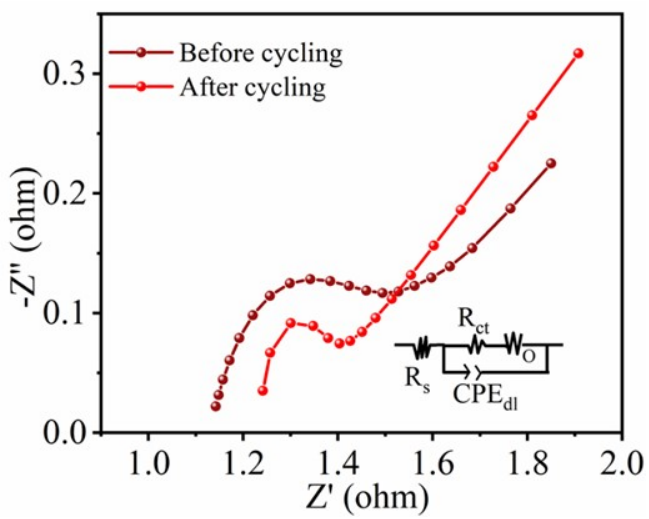

Figure S6. Nyquist plots of CNZS-3 before and after stability test along with the corresponding equivalent circuit.

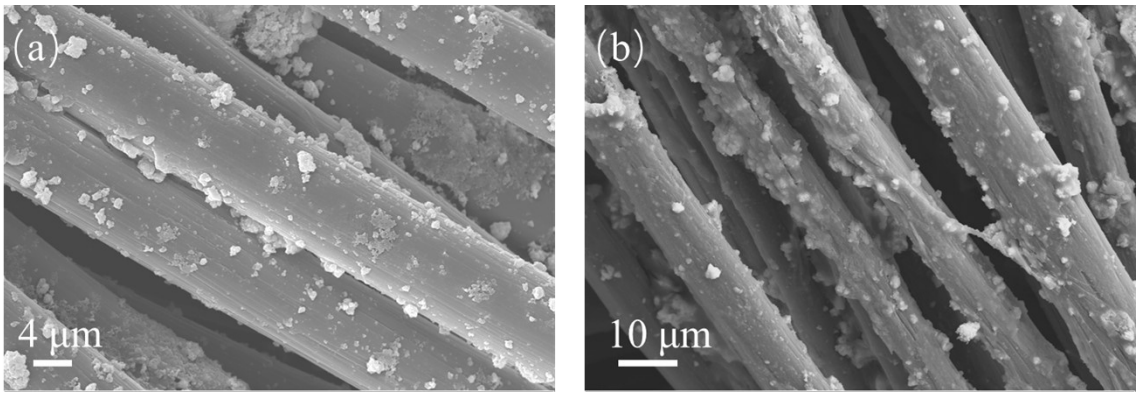

Figure S7. (a, b) SEM images of CNZS-3 electrode before and after cycling in the three-electrode system.

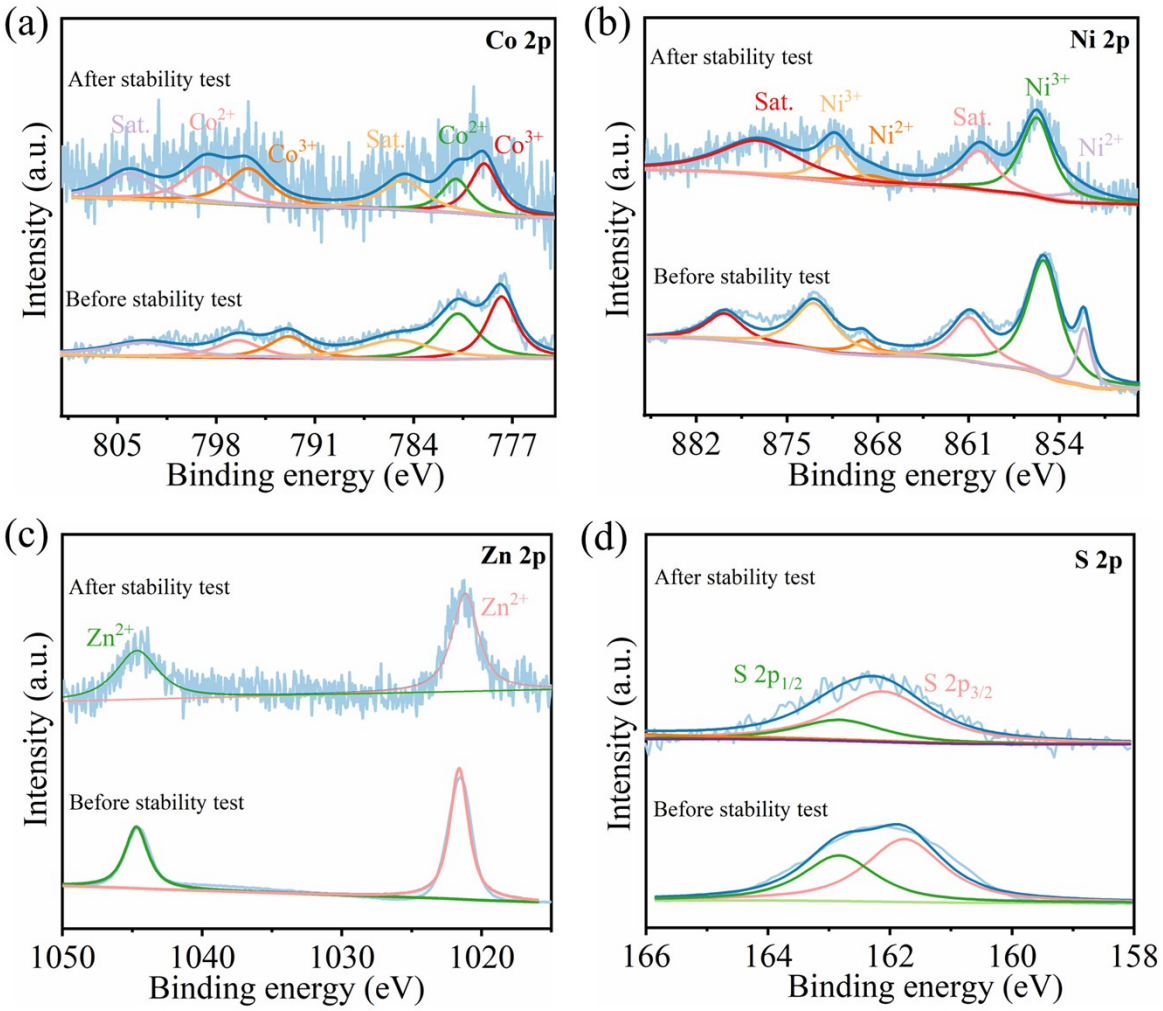

Figure S8. XPS spectra of (a) Co 2p; (b) Ni 2p; (c) Zn 2p; (d) S 2p for CNZS-3 electrode before and after cycling in the three-electrode system.

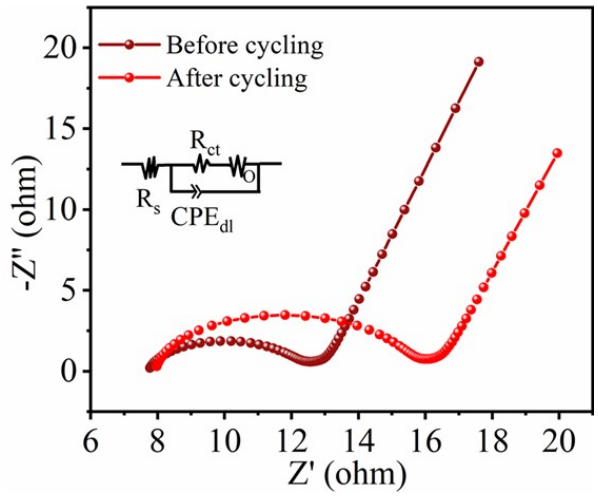

Figure S9. Nyquist plots of the fabricated CNZS-3//AC FSAS device before and after stability test along with the corresponding equivalent circuit.

Tables:

Table S1. The molar ratios of CNZS.

Samples	$Co(NO_3)_2$ (mmol)	$Ni(NO_3)_2$ (mmol)	$Zn(CH_3COO)_2$ (mmol)	CH_4N_2O (mol)	NH_4F (mol)
CNZS-1	0.8	1.95	0.2	0.05	0.02
CNZS-2	0.8	1.85	0.3	0.05	0.02
CNZS-3	0.8	1.75	0.4	0.05	0.02
CNZS-4	0.8	1.65	0.5	0.05	0.02

Table S2. The specific surface area of CNZS.

Samples	Specific surface area (m^2 g^{-1})
CNZS-1	39.13
CNZS-2	41.95
CNZS-3	94.81
CNZS-4	63.43

Table S3. Quantitative mapping of the SEM EDS shown in Figure 2d.

Element	Weight %	Atomic %
S K	34.38	49.42
Co K	23.99	18.76
Ni K	30.95	24.29
Zn K	10.68	7.53
Totals	100.00	

Table S4. The XPS fitting area ratio of Co and Ni.

Samples	Fitting data	Co^{2+}	Co^{3+}	Ni^{2+}	Ni^{3+}
CNZS-1	Fitting area	27506	10534	5038	156846
		12434	4962	7313	70251
	Fitting area ratio	72%	28%	5%	95%
CNZS-2	Fitting area	9816	11354	3521	60413
		4333	5595	7502	29908
	Fitting area ratio	45%	55%	10%	90%
CNZS-3	Fitting area	12313	11354	5800	48695
		5285	5595	10441	24589
	Fitting area ratio	49%	51%	18%	82%
CNZS-4	Fitting area	10958	7957	7345	25218
		5445	3973	11632	13819
	Fitting area ratio	57%	43%	33%	67%

Table S5. Parameters of the proposed equivalent circuit model.

Samples	R_s (Ω)	R_{ct}(Ω)	W_o-R	CPE-P
CNZS-1	1.031	1.7380	4.507	1.272
CNZS-2	0.9775	0.6480	1.638	0.9623
CNZS-3	1.245	0.2765	1.002	0.7010
CNZS-4	1.271	0.5065	0.9011	1.016
CNZS-3 (After cycling)	1.031	0.40165	1.051	1.034

Table S6. Electrochemical performance indices of CNZS compared with previously reported works.

Materials	Specific capacitance	Rate capability	Capacitance retention	Ref.
$(Co,Ni,Zn)_9S_8$	1664 F g^{-1} at 1 A g^{-1} (231 mAh g^{-1} at 1 A g^{-1})	1391 F g^{-1} at 20 A g^{-1}	95% (10,000 cycles)	This work
CoZnNiS	1349.2 F g^{-1} at 1 A g^{-1}	927.8 F cm^{-3} at 10 A g^{-1}	90.6% (10,000 cycles)	1
Au/ZnCoNi-S	302.6 mAh g^{-1} at 1 A g^{-1}	212.8 mAh g^{-1} at 10 A g^{-1}	91.2% (10,000 cycles)	2
Zn-Ni-Co-S/Zn-Ni-Co-O	1445 C g^{-1} at 1 A g^{-1}	1228 C g^{-1} at 20 A g^{-1}	86.1% (3,000 cycles)	3
$(Fe,Co,Ni)_9S_8$	134.7 mAh g^{-1} at 1 A g^{-1}	580 F g^{-1} at 10 A g^{-1}	80.5% (10,000 cycles)	4
CoZnS	1288 F g^{-1} at 2 mA cm^{-2}	1239 F g^{-1} at 6 mA cm^{-2}	85% (5,000 cycles)	5
rGO/ZnCoS	891 F g^{-1} at 1 A g^{-1}	709 F g^{-1} at 5 A g^{-1}	99% (5,000 cycles)	6
Ni-Zn-S	400 F g^{-1} at 0.7 A g^{-1}	240 F g^{-1} at 10 A g^{-1}	97% (2,000 cycles)	7
$NiZn_2O_4@NiZn_2S_4$	1588 C g^{-1} at 1 A g^{-1}	983 C g^{-1} at 6 A g^{-1}	86.9% (10,000 cycles)	8
$NiCo_2S_4$	455 F g^{-1} at 1 A g^{-1}	196 F g^{-1} at 4 A g^{-1}	95.1% (10,000 cycles)	9
$NiCo_2S_4$	154.1 mAh g^{-1} at 2 A g^{-1}	124.86 mAh g^{-1} at 15 A g^{-1}	95.2% (5,000 cycles)	10

Table S7. Parameters of the proposed equivalent circuit model on the fabricated CNZS-3//AC FSAS device before and after stability.

Samples	R_s (Ω)	R_{ct} (Ω)	W_o-R	CPE-P
Before cycling	7.721	4.424	2.503	0.874
After cycling	7.934	5.470	3.045	0.941

Table S8. Performance comparison of as-assembled (Co, Ni, Zn)$_9$S$_8$//AC and previous reported sulfide-based devices.

Devices	Specific capacitance	Energy density	Ref.
(Co, Ni, Zn)$_9$S$_8$//AC	1664 F g^{-1} at 2 A g^{-1}	66.67 Wh kg^{-1} at 1500 W kg^{-1}	This work
Ni-Co-Mn sulfides//Active Carbon	124 F g^{-1} at 2 A g^{-1}	49.8 Wh kg^{-1} at 1700 W kg^{-1}	11
NiS@SnS@$Ni_3Sn_2S_2$//Active Carbon	766 F g^{-1} at 1 A g^{-1}	85.2 Wh kg^{-1} at 3600 W kg^{-1}	12
MnCoP@NiF//Active Carbon@NiF	291 mA h g^{-1} at 1 A g^{-1}	57.0 Wh kg^{-1} at 800 W kg^{-1}	13
$NiCo_2S_4$/Co_9S_8//Active Carbon	371 F g^{-1} at 0.5 A g^{-1}	17.4 Wh kg^{-1} at 181 W kg^{-1}	14
rGO/NiCoS// Active Carbon	665.6 C g^{-1} at 2 A g^{-1}	47.2 Wh kg^{-1} at 1600 W kg^{-1}	15
CuS/Co_3S_4//Active Carbon	1483 F g^{-1} at 1 A g^{-1}	55 Wh kg^{-1} at 373 W kg^{-1}	16
MoS_2@CdS@GO//Active Carbon	1226 F g^{-1} at 1 A g^{-1}	41 Wh kg^{-1} at 587 W kg^{-1}	17
Cu_2CoSnS_4//Active Carbon	394 F g^{-1} at 0.7 A g^{-1}	-	18

References

[1] Y. Liu, N. Xin, Q. Yang, W. Shi, 3D CNTs/graphene network conductive substrate supported MOFs-derived CoZnNiS nanosheet arrays for ultra-high volumetric/gravimetric energy density hybrid supercapacitor, *J. Colloid Interface Sci*., 2021, **583**, 288-298.

[2] S. Yang, M. Xiao, M. Xiao, W. Zhang, X. Niu, X. Du, X. Hui, Z. Song, X. Gao, The enhanced properties of ZnCoNi-S electrode by magnetron sputtering of Au nanoparticles for high performance supercapacitors, *J. Power Sources*, 2024, **623**, 235424.

[3] Y. Zhang, L. Huang, X. Lei, H. Huang, W. Guo, S. Wang, Hierarchical ternary Zn-Ni-Co sulfide/oxide heterostructure for high specific energy hybrid supercapacitor, *J. Alloys Compd.*, 2023, **962**, 171201.

[4] N. Liu, Z. Peng, Y. Tian, H. Liu, Y. Zhang, D. V. Deyneko,L. Mei, Cobalt pentlandite structured $(Fe,Co,Ni)_9S_8$: Fundamental insight and evaluation of hybrid supercapacitor, *Appl. Surf. Sci.*, 2023, **611**.

[5] G. Chavan, A. Sikora, R. Pawar, J. Warycha, P. Morankar, C.-W. Jeon, Hierarchical framework of CoZnS as a high-performance electrode material for supercapacitors, *Ceram. Int.*, 2023, **49**, 282-293.

[6] M. Manikandan, D. K. Kulurumotlakatla, E. Manikandan, K. Karthigeyan, A. A. Al-Kahtani, Hydrothermal synthesis of rGO/ZnCoS composite for high performance asymmetric supercapacitor and HER applications, *J. Energy Storage*, 2023, **72**, 108769.

[7] F. E.-T. Heakal, A. A. Elkholy, S. Ahmed, Simple and affordable synthesis of a binder-free nickel-zinc sulfide electrode for high-performance supercapacitors, Inorg. *Chem. Commun.*, 2024, **163**, 112356.

[8] X. Min, B. Wen, J. Feng, X. Lin, Nanosheet@nanosheet $NiZn_2O_4$@$NiZn_2S_4$ core-shell mesoporous heterostructure as an electrode material for aqueous hybrid supercapacitors, *J. Energy Storage*, 2024, **81**, 110410.

[9] S. Ramesh, K. Karuppasamy, D. Vikraman, H. Yadav, H.-S. Kim, A. Sivasamy, H. S. Kim, Fabrication of $NiCo_2S_4$ accumulated on metal organic framework nanostructured with multiwalled carbon nanotubes composite material for supercapacitor application, *Ceram. Int.*, 2022, **48**, 29102-29110.

[10] D. K. Kulurumotlakatla, A. K. Yedluri,H.-J. Kim, Hierarchical $NiCo_2S_4$ nanostructure as highly efficient electrode material for high-performance supercapacitor applications, *J. Energy Storage*, 2020, **31**, 101619.

[11] C.Z.Wei,Q.Y. Chen, C. Chen, R. Liu, Q. Zhang, L.P. Zhang, Mesoporous nickel cobalt manganese sulfide yolk–shell hollow spheres for high-performance electrochemical energy storage, *Inorg. Chem. Front*., 2019, **6**, 1851-1860.

[12] V. Gayathri, V. Ragavendran, N. Rajamanickam, J. Mayandi, P. Nithiananthi, Mixed phase nanoarchitectonics of NiS@SnS@$Ni_3Sn_2S_2$ as a tetrafunctional catalyst for dye-sensitized solar cells, supercapacitors, and water splitting applications, *J. Energy Storage*, 2023, **70**, 107952.

[13] M. Shirvani, S.S.H. Davarani, Self-templated construction of hollow trimetallic MnNiCoP yolk–shell spheres assembled with nanosheets as a satisfactory positive

electrode material for hybrid supercapacitors, *Nanoscale*, 2023, 15, 11115-11130.
[14] R.R. Neiber, J. Kumar, R.A. Soomro, S. Karkus, H.M. Abo-Dief, A.K. Alanazi, Z.M. El-Bahy, $NiZnCoO_4/CoWO_4$ hybrid composite with improved electrochemical performance for supercapacitor application, *J. Energy Storage*, 2022, **52**, 104900.
[15] T.P. Manh, N.N. Van, V.B.T. Phung, L.N. Thi, Q.N. Quy, N.T. Van, One-step preparation of Ni-Co binary metal sulfides on reduced graphene oxide for all-solid-state supercapacitor devices with enhanced electrochemical performance, *Ceram. Int.*, 2024, **50**, 22757-22770.
[16] T. Pang, M. Luo, X. Liu, Y. Zhang, T. Zhao, P. Shi, F. Li,. Microflower-like CuS/Co_3S_4 composite as high-capacity and excellent-stability material for hybrid supercapacitors, *J. Alloys Compd.*, 2024, 1008, 176563.
[17] S. Irfan, M. Aalim, M.H. Flaifel, I. Nazir, M.A. Shah, M.Q. Lone, G.N. Dar, Enhanced electrochemical performance of MoS_2@CdS@GO ternary heterostructures for asymmetric supercapacitors, *J. Energy Storage*, 2025, **106**, 114788.
[18] W. Wu, X. Wang, Y. Yan, X.F. Li. Metal-organic frameworks derived porous Cu_2CoSnS_4 ternary metal sulfides for high-performance supercapacitor electrodes, *Mater. Lett.*, 2023, **334**, 133722.